Macroscopic effects for quantum control of broadband isolated attosecond pulse generation with a two-color field

Pengfei Lan, Peixiang Lu,* Qianguang Li, Fang Li, Weiyi Hong, and Qingbin Zhang
Wuhan National Laboratory for Optoelectronics and School of Optoelectronics Science and Engineering, Huazhong University of Science and Technology, Wuhan 430074, People's Republic of China
(Received 1 December 2008; published 16 April 2009)

With a theoretical model including both the single-atom and collective responses to the two-color laser field, we investigate the influence of macroscopic effects on the generation of isolated attosecond pulse. It is shown that broadband supercontinuous high harmonics can be produced by controlling the ionization or acceleration step of high-order harmonic generation (HHG). Utilizing the broadband supercontinuum, isolated sub-100 attosecond pulse can be generated. We also investigate the influence of atomic density on the enhancement of HHG. Moreover, the distortion and dephasing of two-color field in the propagation of ionized gas medium are also discussed.

DOI: 10.1103/PhysRevA.79.043413 PACS number(s): 32.80.Qk, 32.80.Wr, 42.65.Re, 42.65.Ky

I. INTRODUCTION

The production of attosecond pulses in recent years [1–3] has allowed one study the ultrafast processes on the attosecond time scale, shedding light on the electronic dynamics in atoms and molecules for the first time [3–5]. Attosecond pulses are synthesized with high harmonics generated in the interaction of strong laser field and atomic or molecular gas. The process of high harmonic generation (HHG) is well understood in terms of the three-step model [6]. In detail, the electron first tunnels through the potential barrier. Subsequently the free electron is accelerated in the laser field, finally recombines with the parent ion and releases its kinetic energy via emitting high harmonics. Such a process periodically occurs every half optical cycle of the laser field and produces two attosecond pulses in each optical cycle [1]. Thus quantum control of HHG within a fraction of optical cycle is required for the generation of isolated attosecond pulse.

HHG can be controlled via manipulating different steps. Phase-stabilized few-cycle laser pulse is a powerful tool for controlling the electron motion, i.e., the second step of HHG. In a few-cycle laser pulse, the highest harmonics are confined in the half cycle at the highest peak of laser pulse and then isolated attosecond pulse can be produced by the highest harmonics in the cutoff [2,3]. By decreasing the laser-pulse duration, the bandwidth of cutoff can be broadened and the attosecond pulse duration can be compressed [7].

On the other hand, the recombination probability of electron with the parent ion depends sensitively on the polarization of laser field [8]. Therefore, the modulation of laser polarization allows one to control the recombination, i.e., the third step of HHG [9,10]. This scheme, usually called polarization gating, has successfully controlled the HHG within a half cycle of laser field and produces an isolated attosecond pulse [11].

Another way to control HHG is the two-color field scheme [12–18]. By mixing a control laser pulse to the fundamental pulse, the synthesized field can be shaped. Then electron motion (the second step of HHG) as well as HHG can be controlled by the two-color field. Pfeifer *et al.* [14] pointed out that isolated attosecond pulse can be produced with a multicycle (24 fs) two-color pulse. Lan *et al.* [15] and Zeng *et al.* [16] proposed to generate an isolated sub-100 attosecond pulse by mixing a second-harmonic pulse to the few-cycle (~5 fs) fundamental field. Lan *et al.* [15] also showed that the driving laser pulse can be increased to 10 fs by mixing a subharmonic pulse to the fundamental field. On the other hand, the two-color field also can control the tunnel ionization [17], i.e., the first step of HHG. With a shaped two-color field, tunnel ionization can be confined within a fraction of optical cycle and broadband isolated attosecond pulse can be produced by the high harmonics in the plateau. But these works [12,14–18] only considered the single-atom response to the two-color field. For the real scenario, a full description of HHG requires not only the laser-atom interaction at the microscopic level, but also the propagation of driving field and high harmonics through the gas medium at the macroscopic level. Particularly, phase matching in the propagation plays an important role in HHG [19–23]. Moreover, the propagation through ionized gas medium will lead to a distortion and phase shift of the driving field [22]. This effect becomes a very serious issue in the two-color field scheme. It is because HHG depends sensitively on the relative phase of two-color field [14–17]. But due to different intensity and frequency, the distortion and phase shift induced by ionized gas are different for the fundamental and control laser fields. It may result in a dephasing of two-color field and induce a significant influence or even destroy the isolated attosecond pulse reported at the single-atom level [14–17]. Therefore, in this work, we investigate the influence of macroscopic effects on the generation of isolated attosecond pulse in two-color field.

The paper is organized as follows. In Sec. II, we describe the theoretical model including the single-atom response and the macroscopic effects. In Sec. III, the results are presented and discussed. In Sec. III A, we first discuss the control of ionization (the first step of HHG) with two-color field, while in Sec. III B, we discuss the control of acceleration (the sec-

*Corresponding author; lupeixiang@mail.hust.edu.cn

ond step of HHG). The results are finally summarized in Sec. IV.

II. THEORETICAL MODEL

The simulation is carried out by taking into account both the single-atom response to the laser pulse and the collective response of macroscopic gas to the laser and high harmonic fields. The two-color laser field is

$$E_l = E_0 + E_1 = A_0 \exp[-2\ln 2(t-T/2)^2/\tau^2]\{\cos[\omega_0(t-T/2)] + \sqrt{\alpha}\cos[2\omega_0(t-T/2)+\phi]\}, \quad (1)$$

where E_0 and E_1 are the fundamental and control fields, respectively, A_0 and ω_0 are the amplitude and frequency of the fundamental field, $2\omega_0$ is the frequency of the control field, α and ϕ are the relative intensity and phase between the control and fundamental fields, and τ is the pulse duration. The laser pulse is centered at $T/2$, where $T=12T_0$ and T_0 is the optical cycle of fundamental laser pulse. The single-atom response is calculated with the Lewenstein model [24] and the nonlinear dipole momentum is [in atomic units (a.u.)]

$$d_{nl} = i\int_{-\infty}^{t} dt' \left(\frac{\pi}{\epsilon + i(t-t')/2}\right)^{1.5} d^*[p_{st}(t',t)-A(t)]d[p_{st}(t',t) - A(t')]\exp[-iS_{st}(t',t)]E(t')|a(t)|^2 + \text{c.c.} \quad (2)$$

In this equation, $E(t)$ is the electric field, $A(t)$ is the vector potential, ϵ is a positive regularization constant, and $|a(t)|^2$ is the depletion of ground state. The ground-state amplitude $a(t)$ can be expressed as

$$a(t) = \exp\left(-\int_{-\infty}^{t} \eta(t'')dt''\right), \quad (3)$$

where

$$\eta(t) = \int d^3p \int_{-\infty}^{t} dt' E^*(t) d^*[p-A(t)]E(t')d[p-A(t')] \times \exp[-iS(t,t')]. \quad (4)$$

As demonstrated in [24], the above equation can be analyzed using the saddle-point method, then one can recover the tunneling ionization rate obtained by the Ammosov-Delone-Krainov (ADK) theory [25]. Note that $|a(t)|^2$ can be neglected if the ground-state depletion is insignificant (for instance, in Fig. 2, the ionization rate is less than 0.001). $d(p)$ in Eq. (2) is the field free dipole transition matrix element between the ground state and the continuum state,

$$d(p) = i\frac{2^{7/2}}{\pi}(2I_p)^{5/4}\frac{p}{(p+2I_p)^3}, \quad (5)$$

where I_p is the ionization energy of target gas. p_{st} and S_{st} are the stationary momentum and quasiclassical action, respectively. Their values are

$$p_{st}(t',t) = \frac{1}{t-t'}\int_{t'}^{t} A(t'')dt'', \quad (6)$$

$$S_{st}(t',t) = (t-t')I_p - p_{st}^2(t',t)(t-t')/2 + \int_{t'}^{t} A^2(t'')dt''/2. \quad (7)$$

To simulate the collective response of macroscopic gas, we solve the light propagation for the laser and high harmonic fields in cylindrical coordinate separately [22,23,26],

$$\nabla^2 E_l(r,z,t) - \frac{1}{c^2}\frac{\partial^2 E_l(r,z,t)}{\partial t^2} = \frac{\omega_p(r,z,t)^2}{c^2}E_l(r,z,t), \quad (8)$$

$$\nabla^2 E_h(r,z,t) - \frac{1}{c^2}\frac{\partial^2 E_h(r,z,t)}{\partial t^2} = \frac{\omega_p(r,z,t)^2}{c^2}E_h(r,z,t) + \mu_0\frac{\partial^2 P_{nl}(r,z,t)}{\partial t^2}, \quad (9)$$

where E_l and E_h are the laser field and high harmonics, respectively. ω_p is the plasma frequency and is given by [23,26]

$$\omega_p = e\sqrt{\frac{n_e(r,z,t)}{m\epsilon_0}}. \quad (10)$$

The nonlinear polarization of gas is $P_{nl}=n_0 d_{nl}$. n_0 and n_e are the densities of neutral atoms and free electrons. The electron density can be expressed as

$$n_e(t) = n_0\left[1-\exp\left(-\int_{-\infty}^{t} w(t')dt'\right)\right], \quad (11)$$

where $w(t')$ is the ionization rate calculated with ADK theory. As demonstrated by Brabec and Krausz [27], ADK theory can well predict the ionization rate in the tunnel ionization regime characterized by $\gamma<1$ and $E_l<E_{bs}$. Here γ is the Keldysh parameter and E_{bs} is the external field strength suppressing the peak of the Coulomb potential to $-I_p$. These conditions are satisfied in our work. Furthermore, the electronic dynamics of tunnel ionization were experimentally investigated recently [28]. It is shown that the ionization rate calculated with ADK theory also agrees well with the experiment in the few-cycle regime. These investigations indicate the validity of ADK theory. Note that this propagation model takes into account both the temporal plasma-induced phase modulation and the spatial plasma lensing effects, but does not consider the atomic dispersion and absorption of high harmonics. As shown in [23], the dispersion and absorption are negligible for neon gas at a density of 1.3×10^{18} cm^{-3} (corresponding a gas pressure of 40 torr). Here we consider helium gas, whose absorptive parameter around 60 eV ($\sim$40th harmonic) is less than 15% of neon and is even less for higher order harmonics [29,30]. This absorption feature indicates that the dispersion and absorption of helium should be negligible for a density less than 1×10^{19} cm^{-3}.

Following the procedure in [23], we change to the moving coordinate frame ($z'=z$ and $t'=t-z/c$) and eliminate the temporal derivative in Eqs. (8) and (9) with Fourier transform, obtaining the equation

$$\nabla^2 \tilde{E}_l(r,z',\omega) - \frac{2i\omega}{c}\frac{\partial \tilde{E}_l(r,z',\omega)}{\partial z'} = \tilde{G}_l(r,z',\omega), \quad (12)$$

$$\nabla^2 \tilde{E}_h(r,z',\omega) - \frac{2i\omega}{c}\frac{\partial^2 \tilde{E}_h(r,z',\omega)}{\partial z'} = \tilde{G}_h(r,z',\omega) - \omega^2 \mu_0 \tilde{P}_{nl}(r,z',\omega). \quad (13)$$

In the above equations, $\tilde{E}_l$, $\tilde{E}_h$, $\tilde{G}_l$, $\tilde{G}_h$, and $\tilde{P}_{nl}$ are the Fourier transforms of E_l, E_h, $\omega_p^2 E_l/c^2$, $\omega_p^2 E_h/c^2$, and P_{nl} on the temporal coordinate. To solve Eqs. (12) and (13), we use the operator-splitting method as [26], which separates the diffraction action and nonlinearity action. Then, Eq. (12) is split to two equations

$$\frac{2i\omega}{c}\frac{\partial \tilde{E}_l(r,z',\omega)}{\partial z'} = \nabla^2 \tilde{E}_l(r,z',\omega), \quad (14)$$

$$\frac{2i\omega}{c}\frac{\partial \tilde{E}_l(r,z',\omega)}{\partial z'} = -\tilde{G}_l(r,z',\omega). \quad (15)$$

These equations can be solved with the Crank-Nicholson method [23,26]. Equation (13) is solved using the same method. In the calculation, 2^{13} points are used in time, 100 points are used along the radial direction, and 200 points along the propagation direction. We first assume a Gaussian beam at the initial position and calculate the single-atom response via Eq. (2). Then the plasma frequency, nonlinear polarization, and high harmonics can be easily calculated. Subsequently, we inset the plasma frequency and medium polarization to Eqs. (8) and (9) and obtain the laser field and high harmonics that propagate to the next position. Repeating this procedure, we obtain the final high harmonics at the exit face of the gas medium.

III. RESULTS AND DISCUSSIONS

For comparison, we first briefly discuss HHG in the fundamental laser pulse alone. The dotted line in Fig. 1 shows the macroscopic harmonic spectrum after propagation through a helium gas. The laser intensity I_0 is 6×10^{14} W/cm^2, wavelength is 800 nm, pulse duration is 5 fs, beam waist is 25 μm, and the Rayleigh length is 2.6 mm. The atomic density is isotropic and equal to 2.5×10^{18} cm^{-3}, which corresponds to a gas pressure of about 75 torr. The gas target is 0.5 mm thick and put at 2 mm after the laser focus. From Fig. 1, one can observe the odd high harmonics in the plateau (less than $85\omega_0$) and a continuum in the cutoff (around $87\omega_0$). This feature can be attributed to the electron motion controlled by the few-cycle laser pulse. As shown in Fig. 2 (dotted line), the atom is predominantly ionized at the peaks P_1, P_2, and P_3 in the fundamental field alone. Then three quantum trajectories contribute to the harmonics in the plateau and the interference of these trajectories gives rise to the high harmonic structure. The electron gains the highest energy in the highest peak P_2 and only the highest-energy electron contributes to the harmonics in the cutoff. Thus the cutoff becomes a continuum, from which an isolated attosecond pulse can be generated. But the bandwidth of cutoff is less than 15 eV, which limits the attosecond pulse duration. In the following, we discuss how to control the HHG with two-color field and how to produce a broader supercontinuum and an even shorter isolated attosecond pulse.

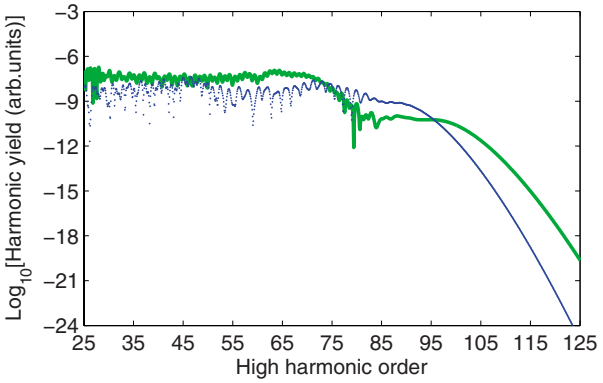

FIG. 1. (Color online) On-axis high harmonics generated by the fundamental pulse alone (dotted line) and ionization gating scheme (solid line) after propagation through a 0.5 mm helium gas. The gas medium is put at 2 mm after the laser focus and the atomic density is 2.5×10^{18} cm^{-3}. The fundamental laser intensity I_0 and wavelength are 6×10^{14} W/cm^2 and 800 nm, respectively. The pulse duration is 5 fs. The relative intensity α and phase ϕ are 4% and 0, respectively.

A. Ionization control with two-color field

We first consider the control of tunnel ionization, i.e., the first step of HHG, with two-color field. According to the ADK theory, the tunnel ionization rate is determined by a prefactor times $\exp(-4I_p\sqrt{2I_p}/3/|E(t)|)$. Therefore, the ionization rate depends exponentially on the electric field. For the two-color field, the electric field

$$|E_l(t)| = |E_0(t) + E_1(t)| = \sqrt{E_0^2(t) + E_1^2(t) + 2E_0(t)E_1(t)}. \quad (16)$$

We can see that the synthesized field can be modulated by a very weak control field $E_1(t)$ since the cross term $E_0(t)E_1(t)$ "amplifies" the weak control field by the large component $E_0(t)$. Consequently, the tunnel ionization can be efficiently controlled by the two-color field. Figure 2(a) shows the electric field of the fundamental (dotted line) and control (dashed line) fields. The intensity of the fundamental field is 6×10^{14} W/cm^2. The intensity of the control field is 4% of the fundamental pulse and the relative phase is 0. As shown in Fig. 2(a), the control field is in the same direction with fundamental field at P_2 and so enhances the ionization. On the contrary, the control field is in the opposite direction with fundamental field at P_1 and P_3 where the ionization is suppressed. Consequently, the ionization is confined in a short interval of 270 attoseconds at P_2 [see the solid line in Fig. 2(a)]. Further, HHG is also confined within half-cycle optical cycle. We name this scheme ionization gating [17]. It should be noted that the laser intensity should be below 8

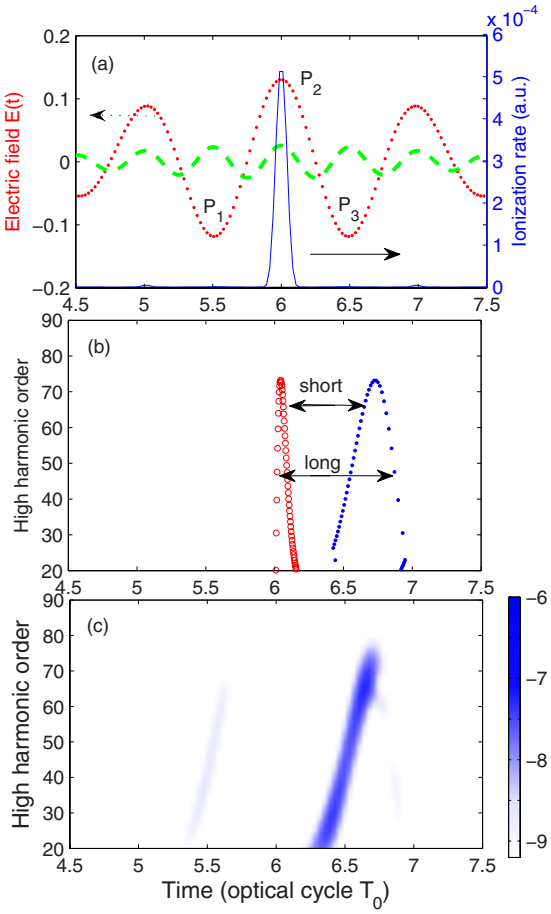

FIG. 2. (Color online) (a) The electric fields of the fundamental laser pulse (dotted line) and its second-harmonic pulse (dashed line). Solid line shows the ionization rate in the two-color field. (b) The classical electron energy is presented as a function of ionization (○) and recombination (●) times. (c) The time-frequency image of the high harmonics shown by the solid line in Fig. 1. The parameters are the same as Fig. 1.

$\times 10^{14}$ W/cm^2 in this scheme. Otherwise, a more intense laser pulse will lead to significant ionization at the leading edge of laser pulse.

The solid line in Fig. 1 shows the high harmonics generated by the ionization gating scheme after propagation through a 0.5 mm helium gas. In contrast to the HHG in the fundamental pulse, the odd harmonic structure in the plateau is removed in the two-color field and a supercontinuum is obtained through the plateau to cutoff. To make clear the underlying physics, we analyze the electron trajectory in the two-color field. In Fig. 2(b), we present the classical electron energy calculated by the three-step model as a function of ionization (○) and recombination (●) times. Note that the three-step model well describes the single-atom response [14,15,17]. We also analyze the quantum trajectory of macroscopic high harmonics with Gabor transform [14,31] and the time-frequency spectrogram is presented in Fig. 2(c). As shown in Fig. 2(b), the single-atom response shows two trajectories, which are the short and long trajectories [6], respectively. After propagation through the gas medium, only the short trajectory survives as shown in Fig. 2(c). It is because the phase matching of short trajectory is preferably achieved by putting the gas target after the laser focus [19,21]. On the other hand, since only the short trajectory survives, the interference between quantum trajectories is removed and the high harmonic spectrum becomes continuous through the plateau to cutoff. The bandwidth is 70 eV, far broader than the cutoff in the fundamental pulse alone. Additionally, we can see from Fig. 1 that the supercontinuous high harmonics generated in the two-color field are more intense than HHG in the fundamental pulse case. It is because the electron is predominantly ionized at P_2 in the two-color field, where the ionization is enhanced as shown in Fig. 2(a). Moreover, one can see from Fig. 2(c) that all the high harmonics in the plateau are emitted almost synchronously, i.e., well phase locked. This feature is in favor of producing a "clean" attosecond pulse [32].

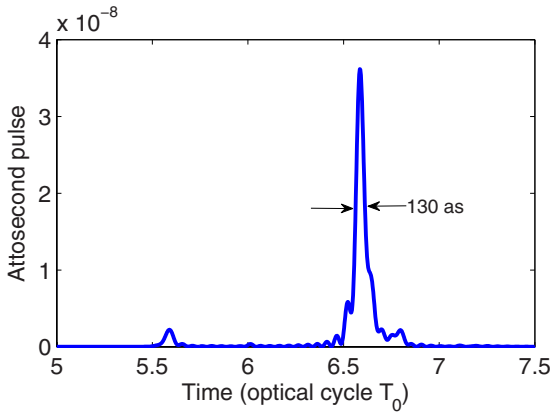

FIG. 3. (Color online) The attosecond pulse generated with the supercontinuous harmonics (40–60 ω_0) shown by the solid line in Fig. 1.

Figure 3 shows the attosecond pulse generated with ionization gating scheme. By synthesizing the harmonics in the plateau (40 to 60 ω_0 shown by the solid line in Fig. 1), an isolated 130 attosecond pulse is obtained. Note also that the bandwidth of supercontinuous high harmonics is 70 eV as shown in Fig. 1. Such a supercontinuum supports an isolated pulse of about 50 attoseconds in the Fourier-transform limit. However, the harmonic chirp prevents producing the Fourier-transform-limited pulse. This issue can be meliorated by a proper filter [11]. For instance, Si filter can transmit the harmonics in the energy range from 40 to 100 eV and also exhibits negative group delay dispersion [33]. Thus Si filter is suitable for compensating the chirp of these harmonics. Note that several other materials, e.g., Sn and Al, also show the similar transition and dispersion features. We may choose proper material depending on the frequency range of interest.

In addition, we consider the influence of atomic density on HHG. Here the atomic density is set below 8×10^{18} cm^{-3} to ensure that the gas absorption is not significant. The solid line in Fig. 4(a) shows the HHG in the ionization gating scheme after propagation through the gas medium with a density of 8×10^{18} cm^{-3} (solid line). The other parameters are the same with Fig. 2. For comparison, HHG for the gas density of 2.5×10^{18} cm^{-3} is also presented in Fig. 4(a) (dashed line). One can see that the high harmonics

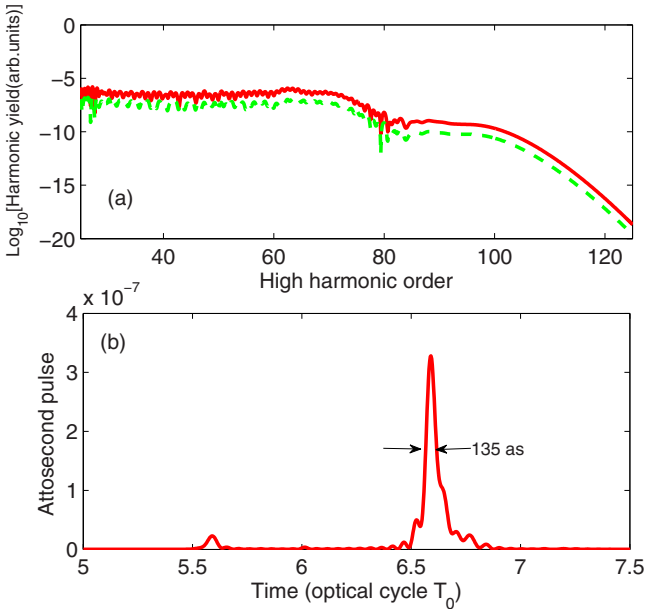

FIG. 4. (Color online) (a) On-axis high harmonics generated in the ionization gating scheme. The atomic densities are 2.5×10^{18} cm^{-3} (dashed line) and 8×10^{18} cm^{-3} (solid line), respectively. Other parameters are the same as Fig. 1. (b) The attosecond pulse generated by the supercontinuous harmonics (40–60 ω_0) shown by the solid line in (a).

are significantly enhanced in the higher density case. When increasing the atomic density from 2.5×10^{18} to 8×10^{18} cm^{-3}, the harmonic intensity is increased by approximately 1 order of magnitude. Moreover, the harmonics in the plateau are also continuous in the higher density case. An isolated 135 attosecond pulse is obtained with the continuous harmonics in the plateau (40 to 60 ω_0) as shown in Fig. 4(b). In contrast to Fig. 3, we can see that the attosecond pulse is also enhanced in the higher density case. We also investigate the influence of laser intensity on HHG. Our calculation shows that the bandwidth of supercontinuous plateau can be slightly increased by increasing the laser intensity to 8×10^{14} $\mathrm{W/cm}^2$ and the high harmonic yield is comparable to that shown in Fig. 1.

B. Acceleration control with two-color field

Next, we consider the control of acceleration, i.e., the second step of HHG, with two-color field. According to the three-step model, the electron kinetic energy in the two-color field is

$$E_k = \frac{1}{2}\left(\int_{t_i}^{t_r}[E_0(t)+E_1(t)]dt\right)^2 = \frac{1}{2}\left[\int_{t_i}^{t_r}E_0(t)dt\right]^2+\frac{1}{2}\left[\int_{t_i}^{t_r}E_1(t)dt\right]^2 + \left[\int_{t_i}^{t_r}E_0(t)dt\right]\left[\int_{t_i}^{t_r}E_1(t)dt\right], \quad (17)$$

where t_i and t_r are the ionization and recombination times,

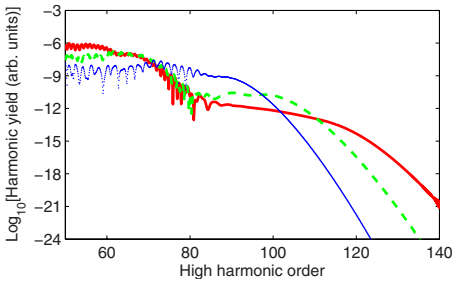

FIG. 5. (Color online) On-axis high harmonics generated in the fundamental field alone (dotted line) and acceleration gating scheme with the relative intensities of 4% (dashed line) and 16% (solid line), respectively. The relative phase ϕ is -0.1π and other parameters are the same with Fig. 1.

respectively. This equation indicates that the electron energy and so high harmonic cutoff can be modulated with the two-color field. Similar to the ionization control case, the control field can be very weak compared to the fundamental field, but the cross term is larger and can significantly modulate the electron energy. By varying the relative phase between the fundamental and control fields, we can increase the electron energy gained in the half cycle P_2 and decrease the energy gained in the half cycles P_1 and P_3. In this way, the cutoff can be broadened and the corresponding attosecond pulse can be compressed. We name this scheme acceleration gating. In contrast to the ionization gating scheme, the acceleration control (i.e., kinetic energy) is determined by the square of the integral of electric field rather than the square of electric field. When the relative phase equal 0, even though the electric field at P_2 is the maximum, the kinetic energy does not reach to the maximum. According to the single-atom response discussed in [15,16], the optimized relative phase is in the range from -0.1π to -0.2π.

Figure 5 shows the high harmonics generated by the acceleration gating scheme after propagation through a 0.5 mm helium gas. The intensity of the fundamental field is 6×10^{14} $\mathrm{W/cm}^2$. The relative intensities between the control and fundamental fields is 4% (dashed line) and 16% (solid line) and the relative phase is -0.1π. Other parameters are the same with Fig. 1. For comparison, the high harmonics generated by the fundamental field alone is also presented in Fig. 5 (dotted line). One can see that the cutoff is blueshifted to 105 ω_0 by mixing a weak control field (dashed line) and the bandwidth of supercontinuum is increased to 40 eV. When the intensity of control field is increased to 16% (solid line in Fig. 5), the cutoff is shifted to 120 ω_0 and the bandwidth of supercontinuum is further broadened to 60 eV. To make clear the underlying physics, we analyze the electron trajectory in the acceleration gating scheme. Figure 6(a) shows the classical trajectory calculated by the three-step model. The parameters are the same with the solid line in Fig. 5. As shown in Fig. 6(a), all the harmonics above 80 ω_0 are confined in the half cycle of P_2. Moreover, both the short and long trajectories are presented in the single-atom response. Similar to the ionization gating case, short trajectory is preferably selected in the propagation. Then only the short trajectory contributes to the macroscopic high harmonics as shown in Fig. 6(b) and the supercontinuous high harmonics

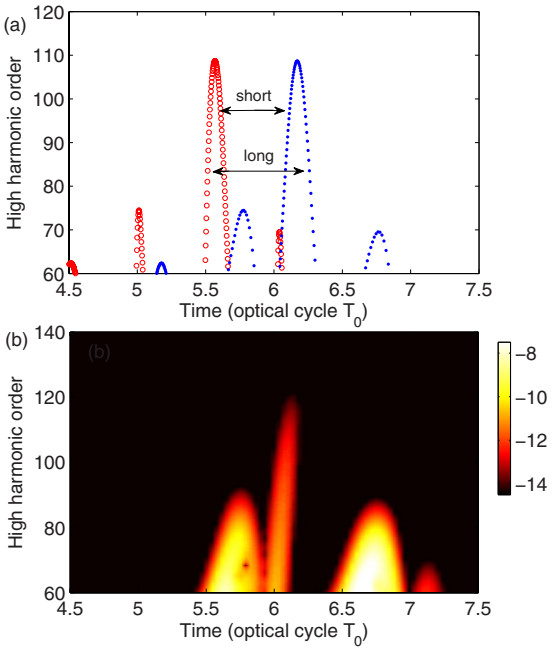

FIG. 6. (Color online) (a) The classical electron energy is presented as a function of ionization (○) and recombination (●) times. (b) The time-frequency image of the high harmonics shown by the solid line in Fig. 5. The parameters are the same with the solid line in Fig. 5.

are emitted almost synchronously. We also analyze the electron trajectory in the acceleration gating scheme with a relative intensity of 4% (corresponding to the dashed line in Fig. 5), which exhibits similar features.

Figure 7 shows the attosecond pulse generated in the acceleration gating scheme. The intensities of the control field are (a) 4% and (b) 16% of the fundamental field and other parameters are the same with Fig. 5. As shown in Fig. 7(a), an isolated 115 attosecond pulse is generated by synthesizing the continuous high harmonics in the cutoff from 80 to 105 ω_0. In contrast to the ionization gating scheme, the attosecond pulse duration is compressed, but the attosecond pulse intensity is lower. It is because the attosecond pulse is generated by the harmonics in the cutoff where the harmonic yield is lower than the harmonics in the plateau. When increasing relative intensity to 16%, the pulse duration is decreased to 105 attoseconds as shown in Fig. 7(b), but the attosecond pulse intensity is further reduced.

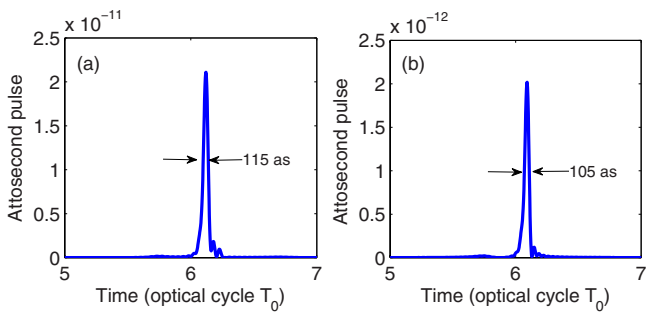

FIG. 7. (Color online) The attosecond pulses generated with the supercontinuous harmonics shown by the (a) solid (80–105 ω_0) and (b) dashed lines (80–110 ω_0) in Fig. 5.

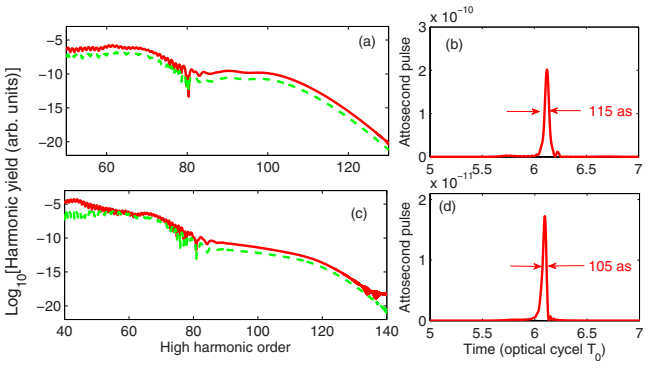

FIG. 8. (Color online) (a) On-axis high harmonics generated in the acceleration gating scheme. The atomic densities are 2.5×10^{18} cm^{-3} (dashed line) and 8×10^{18} cm^{-3} (solid line), respectively. The relative intensity is 4% and other parameters are the same with Fig. 5. (b) The attosecond pulse generated by the supercontinuous harmonics (80–105 ω_0) shown by the solid line in (a). In (c) and (d), the relative intensity is increased to 16% and other parameters are the same with (a) and (b).

Figure 8 shows the influence of atomic density on HHG in the acceleration gating scheme. The solid line in Fig. 8(a) shows the HHG after propagation through the gas with a density of 8×10^{18} cm^{-3}. Other parameters are the same with Fig. 7(a). For comparison, HHG for a gas density of 2.5×10^{18} cm^{-3} is also presented in Fig. 8(a) (dashed line). Similar to the ionization gating scheme, the high harmonics are significantly enhanced in the higher density case. As increasing the atomic density from 2.5×10^{18} to 8×10^{18} cm^{-3}, the harmonic intensity is increased by approximately 1 order of magnitude. Figure 8(b) shows the attosecond pulse generated by the harmonics in the cutoff. One can see that the attosecond pulse intensity is also enhanced in contrast to the lower density case. Figures 8(c) and 8(d) show the high harmonics and attosecond pulse generated in the acceleration gating scheme with the relative intensity of 16%. Similarly, the high harmonic and attosecond pulse yields are significantly enhanced by increasing the atomic density from 2.5×10^{18} to 8×10^{18} cm^{-3}.

To further broaden the supercontinuum and compress the attosecond pulse duration, we investigate HHG in a more intense two-color field. First, we increase the intensity of fundamental field to 1×10^{15} W/cm^2. The intensity of the control field still is 4% (solid line) of the fundamental field and other parameters are the same with Fig. 7(a). The harmonic spectrum and attosecond pulse are shown in Figs. 9(a) and 9(b), respectively. One can see that the bandwidth of supercontinuum is increased to 65 eV [see Fig. 9(a)] and the attosecond pulse duration is reduced to 80 attoseconds [see Fig. 9(b)]. Second, the intensity of fundamental field is kept to be 1×10^{15} W/cm^2 and the intensity of the control field is increased to 16% of the fundamental field. The harmonic spectrum and attosecond pulse are shown in Figs. 9(c) and 9(d), respectively. Clearly, the bandwidth of supercontinuous high harmonics is broadened to 90 eV and an isolated 75 attosecond pulse can be generated. Finally, we increase the intensity of fundamental field to 1.5×10^{15} W/cm^2 and also increase the intensity of the control field to 16% of the fun-

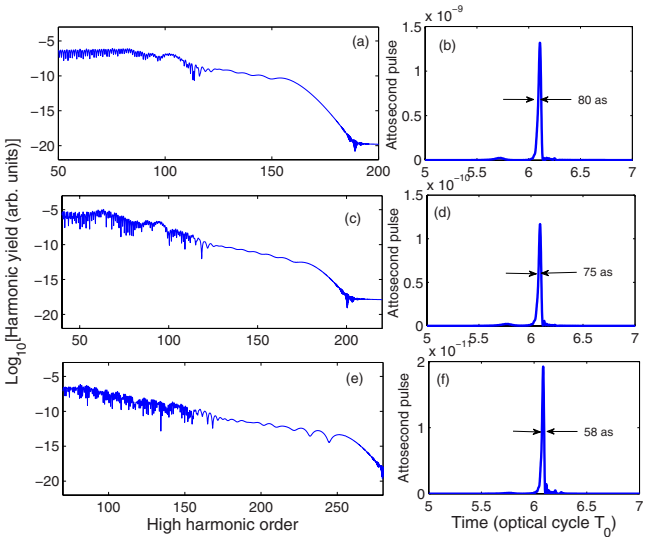

FIG. 9. (Color online) On-axis high harmonics (left column) and attosecond pulses (right column) generated in the acceleration gating scheme. In (a) and (b), $I_0=1\times10^{15}$ W/cm^2, $\alpha=4\%$, and $n_0=2.5\times10^{18}$ cm^{-3}. In (c) and (d), $I_0=1\times10^{15}$ W/cm^2, $\alpha=16\%$, and $n_0=2.5\times10^{18}$ cm^{-3}. In (e) and (f), $I_0=1.5\times10^{15}$ W/cm^2, $\alpha=4\%$, and $n_0=1\times10^{18}$ cm^{-3}. Other parameters are the same with Fig. 5.

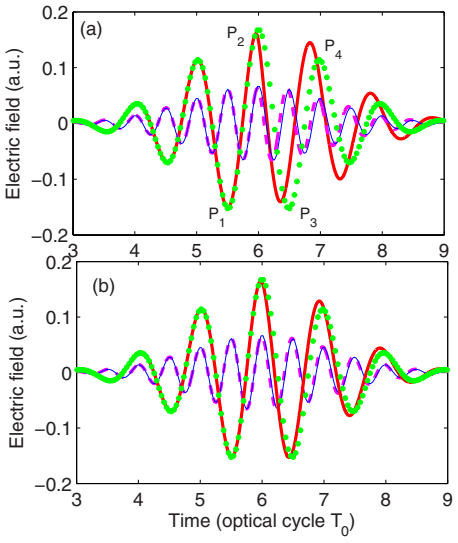

FIG. 10. (Color online) (a) The electric fields of the fundamental and control fields before (dotted and dashed lines) and after propagation (bold and thin solid lines) through a 0.5 mm helium gas. The atomic densities are (a) 8×10^{18} cm^{-3} and (b) 2.5×10^{18} cm^{-3}, respectively. The fundamental laser intensity is 1.0×10^{15} W/cm^2. The relative intensity α and phase ϕ are 16% and 0, respectively.

damental field. As shown in Fig. 9(e), the bandwidth of supercontinuous harmonics is significantly increased to about 140 eV. Then an isolated 58 attosecond pulse is generated as shown in Fig. 9(f).

However, we notice from Fig. 9 that the harmonic spectra decline rapidly from 60 ω_0. The intensity of the supercontinuous high harmonics above 100 ω_0 is decreased more than 3 orders of magnitude. Such a low intensity is a serious disadvantage for the measurement and application of HHG. Moreover, we find that HHG in intense laser field cannot be enhanced by increasing the atomic density. It is because the intense laser field leads to a significant ionization. Then the laser field will be distorted in the propagation through ionized gas medium [22]. This effect is inappreciable in the low-intensity field, but plays an important role in the intense laser field and dense gas medium case. For illustration, we calculate the temporal distortion of laser pulse in the gas medium. Following [22], we focus on the on-axis laser field and adopt the one-dimensional model. Then the light propagation equation is simplified to Eq. (15). Figure 10(a) shows the fundamental and control fields before (dotted and dashed lines) and after (bold and thin solid lines) propagation through a 0.5 mm gas with the density of 8×10^{14} cm^{-3}. The fundamental laser field intensity is 1×10^{15} W/cm^2 and the control field is 16% of the fundamental field. One can observe that the tail of fundamental pulse experiences a notable distortion in the propagation. Peaks P_2 and P_3 are decreased and left shifted; peak P_4 is increased. Additionally, the ionization-induced distortion is different for the fundamental and control fields due to the different intensity and frequency. Consequently, the relative phase and intensity vary in the propagation, which prevents from accurately controlling the HHG. By contrast, the ionization-induced distortion is inappreciable in the gas medium of 2.5×10^{18} cm^{-3} as shown in Fig. 10(b). For a low-intensity field (less than 6×10^{14} W/cm^2), the distortion is negligible after propagation through the gas medium of even 1×10^{19} cm^{-3}. But for the intense field, a low-density gas medium must be adopted to avoid the large distortion. For instance, by increasing the fundamental field intensity to 1.5×10^{15} W/cm^2 (close to the parameters used in [16]), supercontinuum is preserved after propagation through a gas medium of 1×10^{18} cm^{-3} [see Fig. 9(e)]. But for a higher density, ionization induces larger distortion and the supercontinuum will be gradually blurred.

IV. SUMMARY

In summary, we investigate the macroscopic effects for quantum control of isolated attosecond pulse generation with two-color field. We show that the two-color field is a powerful tool for controlling the electron ionization (the first step of HHG) and acceleration (the second step of HHG) processes. In the ionization gating scheme, ionization, and HHG can be confined within half optical cycle and then broadband supercontinuous high harmonics can be generated in the plateau. While in the acceleration gating scheme, broadband supercontinuum can be generated in the cutoff. Compared to the single-atom response, one quantum trajectory can be selected after propagation. We also investigate the influence of atomic density on HHG. The results indicate that a higher gas density is in favor of enhancing the high harmonic yield. But a low-density gas should be adopted in the intense laser field case. Otherwise, significant electrons are produced in the interaction of intense laser field and dense gas. This

effect will induce a large distortion and dephasing of two-color field and prevent from the control of HHG. Moreover, the broadband supercontinuum enables the generation of sub-100 isolated attosecond pulse. In contrast to the acceleration gating case, the ionization gating scheme produces the supercontinuous high harmonics in the plateau and the harmonic and attosecond pulse yields are higher.

ACKNOWLEDGMENTS

This work was supported by the National Natural Science Foundation of China under Grants No. 10774054 and No. 10734080, 973 Program under Grant No. 2006CB806006, and also supported by the State Key Laboratory of Precision Spectroscopy of Huadong Normal University.

[1] P. M. Paul, E. S. Toma, P. Breger, G. Mullot, F. Augé, Ph. Balcou, H. G. Muller, and P. Agostini, Science **292**, 1689 (2001).
[2] M. Hentschel, R. Kienberger, Ch. Spielmann, G. A. Reider, N. Milosevic, T. Brabec, P. Corkum, U. Heinzmann, M. Drescher, and F. Krausz, Nature (London) **414**, 509 (2001).
[3] R. Kienberger, E. Goulielmakis, M. Uiberacker, A. Baltuska, V. Yakovlev, F. Bammer, A. Scrinzi, Th. Westerwalbesloh, U. Kleineberg, U. Heinzmann, M. Drescher, and F. Krausz, Nature (London) **427**, 817 (2004).
[4] M. Drescher, M. Hentschel, R. Kienberger, M. Uiberacker, V. Yakovlev, A. Scrinzi, Th. Westerwalbesloh, U. Kleineberg, U. Heinzmann, and F. Krausz, Nature (London) **419**, 803 (2002).
[5] M. Uiberacker, Th. Uphues, M. Schultze, A. J. Verhoef, V. Yakovlev, M. F. Kling, J. Rauschenberger, N. M. Kabachnik, H. Schröder, M. Lezius, K. L. Kompa, H.-G. Muller, M. J. J. Vrakking, S. Hendel, U. Kleineberg, U. Heinzmann, M. Drescher, and F. Krausz, Nature (London) **446**, 627 (2007).
[6] P. B. Corkum, Phys. Rev. Lett. **71**, 1994 (1993).
[7] E. Goulielmakis, M. Schultze, M. Hofstetter, V. S. Yakovlev, J. Gagnon, M. Uiberacker, A. L. Aquila, E. M. Gullikson, D. T. Attwood, R. Kienberger, F. Krausz, and U. Kleineberg, Science **320**, 1614 (2008).
[8] K. S. Budil, P. Salières, A. L'Huillier, T. Ditmire, and M. D. Perry, Phys. Rev. A **48**, R3437 (1993).
[9] M. Ivanov, P. B. Corkum, T. Zuo, and A. Bandrauk, Phys. Rev. Lett. **74**, 2933 (1995).
[10] I. J. Sola, E. Mévek, L. Elouga, E. Constant, V. Strelkov, L. Poletto, P. Villoresi, E. Benedetti, J. P. Caumes, S. Stagira, C. Vozzi, G. Sansone, and M. Nisoli, Nat. Phys. **2**, 319 (2006).
[11] G. Sansone, E. Benedetti, F. Calegari, C. Vozzi, L. Avaldi, R. Flammini, L. Poletto, P. Villoresi, C. Altucci, R. Velotta, S. Stagira, S. De Silvestri, and M. Nisoli, Science **314**, 443 (2006).
[12] C. Figueira de Morrison Faria and M. L. Du, Phys. Rev. A **64**, 023415 (2001).
[13] Y. Oishi, M. Kaku, A. Suda, F. Kannari, and K. Midorikawa, Opt. Express **14**, 7230 (2006).
[14] T. Pfeifer, L. Gallmann, M. J. Abel, P. M. Nagel, D. M. Neumark, and S. R. Leone, Phys. Rev. Lett. **97**, 163901 (2006).
[15] P. F. Lan, P. X. Lu, W. Cao, Y. H. Li, and X. L. Wang, Phys. Rev. A **76**, 011402(R) (2007).
[16] Z. N. Zeng, Y. Cheng, X. H. Song, R. X. Li, and Z. Z. Xu, Phys. Rev. Lett. **98**, 203901 (2007).
[17] P. F. Lan, P. X. Lu, W. Cao, Y. H. Li, and X. L. Wang, Phys. Rev. A **76**, 051801(R) (2007).
[18] W. Y. Hong, P. X. Lu, P. F. Lan, Z. Y. Yang, Y. H. Li, and Q. Liao, Phys. Rev. A **77**, 033410 (2008).
[19] P. Antoine, A. LHuillier, and M. Lewenstein, Phys. Rev. Lett. **77**, 1234 (1996).
[20] M. Bellini, C. Lynga, A. Tozzi, M. B. Gaarde, T. W. Hänsch, A. L'Huillier, and C.-G. Wahlström, Phys. Rev. Lett. **81**, 297 (1998).
[21] P. Salières, B. Carré, L. Le Déroff, F. Grasbon, G. G. Paulus, H. Walther, R. Kopold, W. Becker, D. B. Milošević, A. Sanpera, and M. Lewenstein, Science **292**, 902 (2001).
[22] M. Geissler, G. Tempea, A. Scrinzi, M. Schnürer, F. Krausz, and T. Brabec, Phys. Rev. Lett. **83**, 2930 (1999).
[23] E. Priori, G. Cerullo, M. Nisoli, S. Stagira, S. De Silvestri, P. Villoresi, L. Poletto, P. Ceccherini, C. Altucci, R. Bruzzese, and C. de Lisio, Phys. Rev. A **61**, 063801 (2000).
[24] M. Lewenstein, Ph. Balcou, M. Yu. Ivanov, A. L'Huillier, and P. B. Corkum, Phys. Rev. A **49**, 2117 (1994); P. Antoine, A. LHuillier, M. Lewenstein, P. Salieres, and B. Carre, *ibid.* **53**, 1725 (1996).
[25] M. V. Ammesov, N. B. Delone, and V. P. Krainov, Sov. Phys. JETP **64**, 1191 (1986).
[26] N. H. Shon, A. Suda, Y. Tamaki, and K. Midorikawa, Phys. Rev. A **63**, 063806 (2001).
[27] T. Brabec and F. Krausz, Rev. Mod. Phys. **72**, 545 (2000).
[28] P. Eckle, A. N. Pfeiffer, C. Cirelli, A. Staudte, R. Döner, H. G. Muller, M. Bütiker, and U. Keller, Science **322**, 1525 (2008).
[29] http://physics.nist.gov/PhysRefData/FFast/html/form.html.
[30] Eiji J. Takahashi, T. Kanai, K. L. Ishikawa, Y. Nabekawa, and K. Midorikawa, Phys. Rev. Lett. **101**, 253901 (2008).
[31] P. F. Lan and P. X. Lu, Phys. Rev. A **77**, 013405 (2008).
[32] Y. Mairesse, A. de Bohan, L. J. Frasinski, H. Merdji, L. C. Dinu, P. Monchicourt, P. Breger, M. Kovacev, T. Auguste, B. Carre, H. G. Muller, P. Agostini, and P. Salieres, Phys. Rev. Lett. **93**, 163901 (2004); P. F. Lan, P. X. Lu, W. Cao, X. L. Wang, and G. Yang, Phys. Rev. A **74**, 063411 (2006).
[33] E. Gustafsson, T. Ruchon, M. Swoboda, T. Remetter, E. Pourtal, R. Lopez-Martens, Ph. Balcou, and A. L'Huillier, Opt. Lett. **32**, 1353 (2007).